J. Fluid Mech. (2013), *vol.* 723, *pp.* 21–39. © Cambridge University Press 2013
doi:10.1017/jfm.2013.99

Low-Reynolds-number flow through two-dimensional shunts

A. Setchi[1],†, A. J. Mestel[2], K. H. Parker[1] and J. H. Siggers[1]

[1]Department of Bioengineering, Imperial College London, London SW7 2AZ, UK
[2]Department of Mathematics, Imperial College London, London SW7 2AZ, UK

(Received 25 August 2012; revised 12 December 2012; accepted 14 February 2013;
first published online 16 April 2013)

Motivated by numerous biological and industrial applications relating to bypasses, mixing and leakage, we consider low-Reynolds-number flow through a shunt between two channels. An analytical solution for the streamfunction is found by matching biorthogonal expansions of Papkovich–Fadle eigenfunctions in rectangular subregions. The general solution can be adapted to model a variety of interesting problems of flow through two-dimensional shunts by imposing different inlet and outlet flux distributions. We present several such flow profiles but the majority of results relate to the particular problem of a side-to-side anastomosis in the small intestine. We consider different flux fractions through the shunt with particular emphasis on the pressure and recirculating regions, which are important factors in estimating health risks pertaining to this surgical procedure.

Key words: biological fluid dynamics, low-Reynolds-number flows

1. Introduction

The human body relies on shunts (also referred to as anastomoses or fistulas) to either regulate the pressure and flow in the system or to bypass sites of high resistance or damage. A side-to-side intestinal anastomosis, in particular, is the surgical procedure of incising two parallel segments of gut and suturing them together (figure 1). It is used to bypass the redundant loop in case of disease (e.g. Crohn's disease) or to achieve long-term weight loss by restricting the uptake of metabolites. It is the preferred procedure in newborns when the gut is small, in older patients when the segments are of different diameters or when the gut is difficult to mobilize because of adhesions. It has a similar, and sometimes higher, success rate compared with alternative surgical procedures (Resegotti *et al.* 2005; Kiran *et al.* 2011), particularly when several shunts are introduced along the two walls.

Although side-to-side anastomosis is a relatively common surgical procedure, there is still a debate in the surgical community regarding the function of the shunts (Joyce *et al.* 2002). Motivated by the need to understand the mechanisms better, we consider a mathematical model of the flow through a side-to-side anastomosis. The small intestine is a convoluted tube of ∼6–7 m in length and has an average radius of ∼1.25 cm. The rheology of the contents depends on the distance from

† Email address for correspondence: asetchi@imperial.ac.uk

https://doi.org/10.1017/jfm.2013.99 Published online by Cambridge University Press

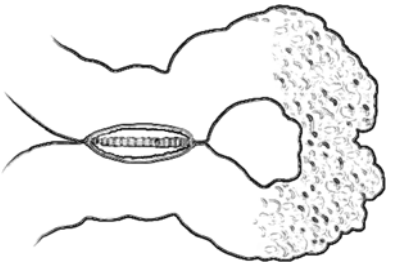


FIGURE 1. A sketch of a side-to-side anastomosis of the small intestine. Drawn after Souba *et al.* (2007).

the stomach. It is semi-liquid as it enters the small intestine from the stomach and the partially digested material leaving it to go into the large intestine has a water content of around 95 %. We model the fluid as Newtonian, so the results should capture the main dynamics if the consumed food is liquefied and we consider the flow a sufficient distance away from the stomach. Although there is some debate about the typical Reynolds number of the flow, it is certainly small (Tripathi 2011). We estimate it as 1.25×10^{-3} based on typical values for density $\rho^d = 1000$ kg m^{-3}, viscosity $\mu^d = 10$ Pa s, length scale $L^d = 2.5$ cm and maximum flow velocity $U^d = 5 \times 10^{-4}$ m s^{-1} (Setchi 2012).

There are several analytical models of Stokes flows in idealized geometries (Pozrikidis 1992; Kim & Karrila 2005) but flow through shunts remains challenging near sharp edges and corners. Unbounded two-dimensional shear flow over a wall with a gap was studied analytically by Smith (1987). In addition, Ko & Jeong (1994) found a solution in the same geometry but driven by a stagnation point flow. More recently, Crowdy & Samson (2010) extended the solutions to flow past a wall with two gaps using complex variable techniques. Davis (1991) considered the three-dimensional flow over a planar wall with a circular orifice. The classical problem of channel flow divided by a semi-infinite barrier introduces additional boundaries, which complicates the solution. When the barrier divides the channel exactly into two halves, the flow can be obtained by solving scalar Wiener–Hopf equations using an intricate factorization (Buchwald & Doran 1965; Foote & Buchwald 1985). When it divides a channel asymmetrically, a solution can be obtained numerically using a Padé approximant technique for a matrix Wiener–Hopf system (Abrahams *et al.* 2008). The Wiener–Hopf technique has also been applied to study the flow in a channel with a finite plate parallel to the walls of the channel by Kim & Chung (1984). A simple model of flow through a shunt is to consider a channel with two semi-infinite barriers with a gap between them as in figure 2; the general solution is determined by the four imposed fluxes at the geometrical inlets/outlets. The parallel boundaries with changing conditions suggest use of the Wiener–Hopf techniques, but the extra boundaries would require a still more complex analysis than that presented by Abrahams *et al.* (2008) and so we choose instead to use the method of Papkovich–Fadle eigenfunctions.

Papkovich–Fadle eigenfunctions were used by Smith (1952) to obtain an exact solution for the normal displacement of a thin semi-infinite strip subjected to arbitrary displacements on the short edge but with the long edges clamped, and convergence of the series was discussed by Joseph (1977), Joseph & Sturges (1978) and Joseph, Sturges & Warner (1982). The method has been used to model two-dimensional Stokes flow in rectangular domains with one inlet and one outlet.

https://doi.org/10.1017/jfm.2013.99 Published online by Cambridge University Press

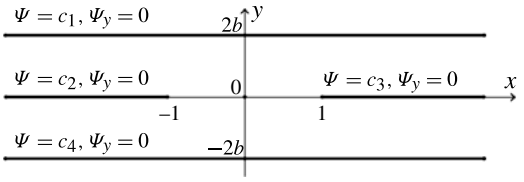


FIGURE 2. Geometry and boundary conditions associated with the streamfunction $\Psi(x, y)$. The constants c_n are determined by the plane Poiseuille flow fluxes at the inlets and outlets.

For example, Joseph & Sturges (1975) studied the liquid circulation in a trench driven by unequal temperatures at the sidewalls. Trogdon & Joseph (1982) used Papkovich–Fadle functions to model flow in an infinite channel over a rectangular slot. Phillips (1989) used the method of matched eigenfunction expansions using Papkovich–Fadle functions to study Stokes flow in a channel with a contraction. A more recent application was by Driesen, Kuerten & Streng (1998), who considered flow over partially covered cavities, and in particular etched holes. Our work is a natural extension to all of these studies as it introduces a geometry with four channel ends rather than two, and thus the resulting matching analysis is more challenging.

We consider a two-dimensional geometry that consists of two channels joined by a slit. This is justified in modelling the small intestine by the fact that the curvature of the vessels during a side-to-side anastomosis is negligible, as the surgery is performed on parallel segments of the gut. The simplified geometry allows an analytical solution of the biharmonic equation. A similar geometry was used in previous work (Setchi *et al.* 2012) for high-Womersley-number flow, in which the flow was governed by Laplace's equation. For that problem, we found qualitative agreement between the results in this geometry and those in the mid-plane of two more realistic three-dimensional geometries: two cylinders joined by a point and two semi-cylinders joined by a rectangular shunt.

In this paper we study Stokes flow in two parallel channels that are connected by a shunt by splitting the domain into rectangular subregions and expressing the flow in each one using Papkovich–Fadle eigenfunction expansions. In § 2 we obtain analytical solutions for the streamfunction in three simplified cases by prescribing the flow fluxes at the inlets and outlets. A particular linear superposition of the three independent solutions is used in § 3 to study a particular problem motivated by side-to-side anastomosis in the small intestine. We briefly discuss other linear combinations in § 4.

2. Mathematical model

Motivated by the problem of low-Reynolds-number flow in a side-to-side anastomosis, we consider Stokes flow in two parallel infinite channels of width $2b$ linked by a side-to-side anastomosis of length 2 (figure 2). Two-dimensional flow can be defined by a streamfunction $\Psi(x, y)$ such that

$$\boldsymbol{u} = \boldsymbol{\nabla} \wedge (\Psi \boldsymbol{k}) \quad \text{or} \quad (u, v) = \left(\frac{\partial \Psi}{\partial y}, -\frac{\partial \Psi}{\partial x} \right), \tag{2.1}$$

where $\boldsymbol{u} = (u, v)$ is the velocity field with respect to the (x, y) coordinate system and $\boldsymbol{k}$ is a unit vector perpendicular to the flow plane. At low Reynolds numbers, the

https://doi.org/10.1017/jfm.2013.99 Published online by Cambridge University Press

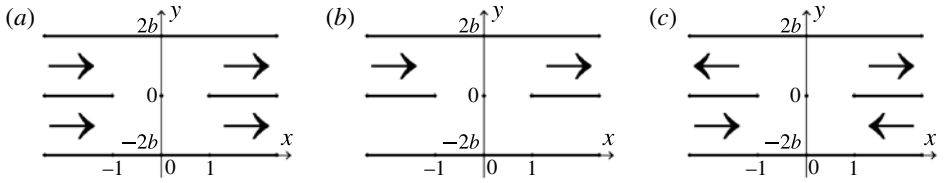


FIGURE 3. A schematic illustrating the three independent Stokes flow solutions: (*a*) the first solution, considered in § 2.1; (*b*) the second solution in § 2.2; (*c*) the third solution in § 2.3. The arrows represent plane Poiseuille flow of maximum velocity 1, corresponding to mean velocity $2/3$ and total volumetric flux $4b/3$, at the extremities.

problem reduces to solving the biharmonic equation

$$\nabla^4 \Psi = 0. \tag{2.2}$$

In this section we solve this problem in the simplified geometry in figure 2 for a general set of fluxes at the inlets and outlets, which are prescribed by the four constants c_1, c_2, c_3 and c_4 in figure 2. In § 3 we will then explore the particular choice $c_1 = c_4$ that corresponds to a model of the flow through an intestinal loop during a side-to-side anastomosis.

We solve (2.2) for a flow that satisfies the boundary conditions of vanishing $\partial\Psi/\partial x$ and $\partial\Psi/\partial y$ at the rigid walls in figure 2. The fluxes at the inlets and outlets are prescribed by c_1, c_2, c_3 and c_4, which provide three constraints, as a constant can be added to Ψ without changing the solution. As in Setchi *et al.* (2012), three linearly independent solutions form a basis for the general case. These three solutions are chosen so as to utilize the lines of symmetry of the geometry. Diagrams of these are shown in figure 3, where the arrows represent plane Poiseuille flow profiles of maximum velocity 1. For each solution we decompose the geometry into a number of simpler rectangular subregions and the streamfunction is represented by means of an expansion of Papkovich–Fadle eigenfunctions in each subregion. The coefficients in these expansions will be obtained by matching them across common interfaces in a weak sense using the biorthogonal properties of these eigenfunctions.

We next describe in detail the aforementioned biorthogonal properties by considering a slightly different problem: solving the biharmonic equation in an infinite channel defined by the boundaries $\eta = \pm 1$. We introduce the Greek variables η and ξ rather than x and y to differentiate between the two geometries in this paper. If we seek separable solutions to the biharmonic equation

$$\left(\frac{\partial^2}{\partial \xi^2} + \frac{\partial^2}{\partial \eta^2}\right)^2 f = 0 \quad \text{with } f = \frac{\partial f}{\partial \nu} = 0 \quad \text{at } \eta = \pm 1, \tag{2.3}$$

then the solutions are linear superpositions of functions of the form $e_1^{(k)}(\eta)\exp(k\xi)$ and $e_2^{(K)}(\eta)\exp(K\xi)$, where

$$e_1^{(k)}(\eta) = k(\cos k \sin(k\eta) - \eta \sin k \cos(k\eta)), \tag{2.4}$$

$$e_2^{(K)}(\eta) = K(\sin K \cos(K\eta) - \eta \cos K \sin(K\eta)). \tag{2.5}$$

The latter are the odd and even Papkovich–Fadle eigenfunctions, respectively. They have the properties that both they and their first derivatives are zero on $\eta = -1$

https://doi.org/10.1017/jfm.2013.99 Published online by Cambridge University Press

and $\eta = 1$ provided that k and K satisfy

$$\sin(2k) = 2k, \tag{2.6}$$

$$\sin(2K) = -2K. \tag{2.7}$$

If k satisfies (2.6) then so do $-\overline{k}$, $-k$ and $\overline{k}$, meaning that the roots in each of the quadrants of the complex plane correspond to one another. We let $S_1 = \{k_1, k_2, \dots\}$ denote the set of roots of (2.6) in the first quadrant, ordered by ascending real part, meaning that the complete set of roots is $\{0\} \cup \{k, -\overline{k}, -k, \overline{k} : k \in S_1\}$. Similarly, the roots of (2.7) are given by $\{0\} \cup \{K, -\overline{K}, -K, \overline{K} : K \in S_2\}$, where $S_2 = \{K_1, K_2, \dots\}$ is the set of roots of (2.7) that lie in the first quadrant ordered by ascending real part. We use e_1^n and e_2^N to denote $e_1^{(k_n)}$ and $e_2^{(K_N)}$, respectively. The Papkovich–Fadle eigenfunctions satisfy the biorthogonality property

$$\langle \boldsymbol{f}_j^N(\eta), \boldsymbol{e}_1^n(\eta)\rangle = -4\sin^4 k_N \delta_{j1}\delta_{nN} \quad \text{for } j = 1, 2;\ \forall n, N \in Z^+, \tag{2.8}$$

$$\langle \boldsymbol{f}_j^N(\eta), \boldsymbol{e}_2^n(\eta)\rangle = -4\sin^4 K_N \delta_{j2}\delta_{nN} \quad \text{for } j = 1, 2;\ \forall n, N \in Z^+, \tag{2.9}$$

where

$$\boldsymbol{e}_1^n(\eta) = \begin{bmatrix} e_1^n(\eta) \\ e_1^{n\prime\prime}(\eta)/k_n^2 \end{bmatrix} \quad \text{and} \quad \boldsymbol{e}_2^n(\eta) = \begin{bmatrix} e_2^n(\eta) \\ e_2^{n\prime\prime}(\eta)/K_n^2 \end{bmatrix}, \tag{2.10}$$

are the eigenvectors, and

$$\boldsymbol{f}_1^n(\eta) = \begin{bmatrix} e_1^n(\eta) + 2\sin k_n \sin(k_n\eta) \\ e_1^n(\eta) \end{bmatrix} \quad \text{and} \quad \boldsymbol{f}_2^n(\eta) = \begin{bmatrix} e_2^n(\eta) - 2\cos K_n \cos(K_n\eta) \\ e_2^n(\eta) \end{bmatrix}, \tag{2.11}$$

are the adjoint eigenvectors (Smith 1952). The two biorthogonal properties (2.8) and (2.9) can be applied to extract coefficients that multiply Papkovich–Fadle eigenfunctions in an equation, similar to the way in which sinusoidal coefficients are extracted in Fourier series using the orthogonality properties of the $\sin(nx)$ and $\cos(mx)$ functions for $n, m \in \mathbb{N}$ and $x \in [0, 2\pi]$.

To ease reading in the later sections, where we apply matching across numerous interfaces, we define the operation

$$\langle \boldsymbol{u}(\eta), \boldsymbol{v}(\eta)\rangle = \int_{-1}^{1} \boldsymbol{u}^{\mathrm{T}} \begin{bmatrix} 0 & -1 \\ 1 & 2 \end{bmatrix} \boldsymbol{v}\, \mathrm{d}\eta \tag{2.12}$$

for any vector functions $\boldsymbol{u}$ and $\boldsymbol{v}$. We also define three new variables

$$y_1 = \frac{y}{b} - 1, \quad y_2 = -\frac{y}{b} - 1, \quad y_3 = \frac{y}{2b} \tag{2.13}$$

so that boundary conditions at $y = 2b$, 0 and $-2b$ can be applied at $y_1 = \pm 1$, $y_2 = \pm 1$ or $y_3 = \pm 1$ depending on the rectangular subregion of interest $[0, 2b]$, $[-2b, 0]$ or $[-2b, 2b]$. Lastly, we introduce the functions

$$\tilde{f}(y) = \frac{y^2}{b} - \frac{y^3}{3b^2} \quad \text{and} \quad f(y_1) = \frac{2b}{3} + by_1 - \frac{by_1^3}{3}, \tag{2.14}$$

which represent plane Poiseuille flow of maximum velocity 1 in a channel with boundaries at $y = 0$ and $y = 2b$.

We now construct the set of three linearly independent flow solutions represented by the diagrams in figure 3. Due to the linearity of the biharmonic equations,

https://doi.org/10.1017/jfm.2013.99 Published online by Cambridge University Press

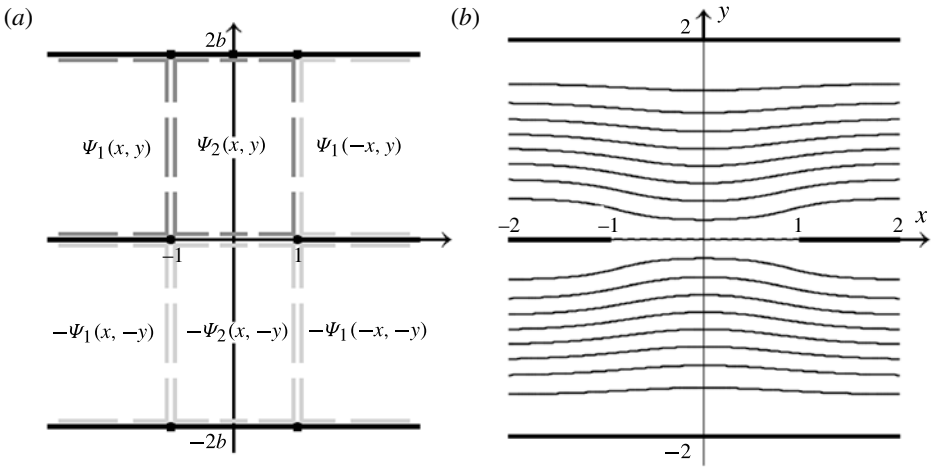


FIGURE 4. (*a*) A diagram of the subregions we consider when constructing the flow profile in figure 3(*a*). (*b*) Streamlines (from left to right) associated with the streamfunction Ψ when the shunt width equals the channel width, i.e. $b = 1$.

a streamfunction $\Psi(x, y)$ can be constructed using appropriate infinite summations of terms that include Papkovich–Fadle eigenfunctions in both the x and y directions. We follow the notation and expansion forms that were used by Smith (1952), as well as the majority of the authors mentioned in the introduction.

2.1. *First solution (parallel flow)*

We first consider a solution to the flow represented in figure 3(*a*); if the shunt were closed, this solution would simply be plane Poiseuille flow from left to right in both channels. The maximum velocity at each end is chosen to be 1, corresponding to the choice $c_1 = 4b/3$, $c_{2,3} = 0$ and $c_4 = -4b/3$ in figure 2. The boundary conditions that need to be satisfied are thus

$$\Psi = \frac{4b}{3} \quad \text{and} \quad \frac{\partial \Psi}{\partial y} = 0 \quad \text{on } y = 2b, \tag{2.15}$$

$$\Psi = 0 \quad \text{and} \quad \frac{\partial \Psi}{\partial y} = 0 \quad \text{on } y = 0, x \leqslant -1 \text{ and } y = 0, x \geqslant 1, \tag{2.16}$$

$$\Psi = -\frac{4b}{3} \quad \text{and} \quad \frac{\partial \Psi}{\partial y} = 0 \quad \text{on } y = -2b, \tag{2.17}$$

$$\Psi \to \tilde{f}(y) \quad \text{as } |x| \to \infty. \tag{2.18}$$

The domain is divided into six subregions (figure 4*a*). As Ψ is even in x and odd in y, it is only necessary to derive the solution in two of the six regions:

$$\Psi(x, y) = \begin{cases} \Psi_1(x, y) & \text{for } x \in (-\infty, -1],\ y \in [0, 2b], \\ \Psi_2(x, y) & \text{for } x \in [-1, 1],\ y \in [0, 2b]. \end{cases} \tag{2.19}$$

https://doi.org/10.1017/jfm.2013.99 Published online by Cambridge University Press

Then we seek solutions using the following expansions:

$$\Psi_1(x, y_1) = f(y_1) + \sum_{n=1}^{\infty} \frac{A_n}{k_n^2} \mathrm{e}^{k_n(x+1)/b} e_1^n(y_1) + \sum_{n=1}^{\infty} \frac{B_n}{K_n^2} \mathrm{e}^{K_n(x+1)/b} e_2^n(y_1), \tag{2.20}$$

$$\Psi_2(x, y_1) = f(y_1) + \sum_{n=1}^{\infty} \frac{C_n}{k_n^2} \frac{\cosh(k_n x/b)}{\cosh(k_n/b)} e_1^n(y_1) + \sum_{n=1}^{\infty} \frac{D_n}{K_n^2} \frac{\cosh(K_n x/b)}{\cosh(K_n/b)} e_2^n(y_1)$$
$$+ \sum_{n=1}^{\infty} \frac{E_n}{b^2 K_n^2} \frac{\cosh(K_n b y_1)}{\cosh(K_n b)} e_2^n(x) + \sum_{n=1}^{\infty} \frac{F_n}{b^2 K_n^2} \frac{\sinh(K_n b y_1)}{\sinh(K_n b)} e_2^n(x) \,. \tag{2.21}$$

It is assumed here and subsequently that complex conjugates are included in the series and all additional notation will be omitted. As the constants k_n and K_n are chosen to have positive real parts only, all terms in the expansions decay exponentially at the outlets except for the plane Poiseuille flow terms. We use eigenfunctions in both the x and y directions in the rectangular region $x \in [-1, 1]$, $y \in [0, 2b]$ with appropriate arguments for different channel widths. All terms in the expansions satisfy the biharmonic equation; therefore, if all boundary conditions and the matching between the subregions are satisfied then the problem is solved. Some boundary conditions are already satisfied by the choice of expansions. The remaining two are

$$\Psi_2 = \frac{4b}{3} \quad \text{and} \quad \frac{\partial \Psi_2}{\partial y} = 0 \quad \text{at } y = 2b. \tag{2.22}$$

If we apply the results of Joseph *et al.* (1982) to our problem, which is defined by the expansions in (2.20)–(2.21) and the boundary conditions in (2.22), we can show that the series will converge uniformly in $x \in (-\infty, \infty) \times y \in [-2b, 2b]$ for both $\Psi(x, y)$ and its first derivatives. We expect that the series for the second and third derivatives will converge non-uniformly near the singularities at the two shunt edges.

At the interface $y = 0$ the first and third derivatives are continuous by construction of the expansions. The other two continuity conditions need to be stipulated and they are equivalent to

$$\Psi_2 = 0 \quad \text{and} \quad \frac{\partial^2 \Psi_2}{\partial y^2} = 0 \quad \text{at } y = 0. \tag{2.23}$$

At the interface $x = -1$ the continuity conditions up to the third derivative of Ψ become

$$\Psi_1 = \Psi_2, \quad \frac{\partial \Psi_1}{\partial x} = \frac{\partial \Psi_2}{\partial x}, \quad \frac{\partial^2 \Psi_1}{\partial x^2} = \frac{\partial^2 \Psi_2}{\partial x^2} \quad \text{and} \quad \frac{\partial^3 \Psi_1}{\partial x^3} = \frac{\partial^3 \Psi_2}{\partial x^3} \quad \text{at } x = -1. \tag{2.24}$$

Substituting the expressions in (2.20)–(2.21) into (2.22)–(2.24) yields, after some algebra, eight equations for the unknown constants in the expansions. Four hold for all x in the range $[-1, 1]$ and four for all y in the range $[0, 2b]$. The system can be transformed into the vector form

$$\sum_{n=1}^{\infty} (E_n + F_n) \boldsymbol{e}_2^n(x) = -\sum_{n=1}^{\infty} \left(F_n \frac{\coth(K_n b) - K_n}{K_n} + E_n \frac{\tanh(K_n b) - K_n}{K_n} \right) \begin{bmatrix} e_2^n(x) \\ 0 \end{bmatrix}, \tag{2.25}$$

https://doi.org/10.1017/jfm.2013.99 Published online by Cambridge University Press

$$\sum_{n=1}^{\infty} \frac{F_n - E_n}{2} \boldsymbol{e}_2^n(x) = \begin{bmatrix} b \\ 0 \end{bmatrix} - \sum_{n=1}^{\infty} \frac{D_n \cos^2 K_n}{\cosh(K_n/b)} \begin{bmatrix} \cosh\left(\dfrac{K_n x}{b}\right) \\ 0 \end{bmatrix} - \sum_{n=1}^{\infty} \frac{C_n \sin^2 K_n}{\cosh(k_n/b)} \begin{bmatrix} \cosh\left(\dfrac{k_n x}{b}\right) \\ 0 \end{bmatrix}, \tag{2.26}$$

$$\sum_{n=1}^{\infty} \frac{C_n - A_n}{2} \boldsymbol{e}_1^n(y_1) + \sum_{n=1}^{\infty} \frac{D_n - B_n}{2} \boldsymbol{e}_2^n(y_1) = \sum_{n=1}^{\infty} \frac{E_n \cos^2 K_n}{\cosh(bK_n)} \begin{bmatrix} \cosh(bK_n y_1) \\ 0 \end{bmatrix} + \sum_{n=1}^{\infty} \frac{F_n \cos^2 K_n}{\sinh(bK_n)} \begin{bmatrix} \sinh(bK_n y_1) \\ 0 \end{bmatrix}, \tag{2.27}$$

$$\sum_{n=1}^{\infty} \frac{k_n \left(A_n + C_n \tanh\left(\dfrac{k_n}{b}\right)\right)}{2b} \boldsymbol{e}_1^n(y_1) + \sum_{n=1}^{\infty} \frac{K_n \left(B_n + D_n \tanh\left(\dfrac{K_n}{b}\right)\right)}{2b} \boldsymbol{e}_2^n(y_1) = \sum_{n=1}^{\infty} \frac{E_n K_n^2}{\cosh(bK_n)} \begin{bmatrix} \cosh(bK_n y_1) \\ 0 \end{bmatrix} + \sum_{n=1}^{\infty} \frac{F_n K_n^2}{\sinh(bK_n)} \begin{bmatrix} \sinh(bK_n y_1) \\ 0 \end{bmatrix}. \tag{2.28}$$

Next we apply the biorthogonality properties by premultiplying both sides of the equations by the dyadic matrix and the adjoint vector of interest. Equations (2.25)–(2.26) for the even eigenfunction in the range $x \in (-1, 1)$ yield two equations for every natural number N:

$$E_N + F_N = \sum_{n=1}^{\infty} \left(F_n \frac{\coth(K_n b) - K_n}{4K_n \cos^4 K_N} + E_n \frac{\tanh(K_n b) - K_n}{4K_n \cos^4 K_N} \right) \left\langle \boldsymbol{f}_2^N(x), \begin{bmatrix} e_2^n(x) \\ 0 \end{bmatrix} \right\rangle, \tag{2.29}$$

$$E_N - F_N = \frac{2b}{\cos^4 K_N} - \sum_{n=1}^{\infty} \frac{D_n \cos^2 K_n}{2\cos^4 K_N} \left\langle \boldsymbol{f}_2^N(x), \begin{bmatrix} \dfrac{\cosh(K_n x/b)}{\cosh(K_n/b)} \\ 0 \end{bmatrix} \right\rangle - \sum_{n=1}^{\infty} \frac{C_n \sin^2 k_n}{2\cos^4 K_N} \left\langle \boldsymbol{f}_2^N(x), \begin{bmatrix} \dfrac{\cosh(k_n x/b)}{\cosh(k_n/b)} \\ 0 \end{bmatrix} \right\rangle. \tag{2.30}$$

Integration of (2.27)–(2.28) between $y = 0$ and $y = 2b$ with respect to the odd eigenfunction yields

$$A_N - C_N = \sum_{n=1}^{\infty} \frac{F_n \cos^2 K_n}{2\sin^4 k_N} \left\langle \boldsymbol{f}_1^N(y_1), \begin{bmatrix} \dfrac{\sinh(bK_n y_1)}{\sinh(bK_n)} \\ 0 \end{bmatrix} \right\rangle, \tag{2.31}$$

$$A_N + C_N \tanh\left(\frac{k_N}{b}\right) = -\sum_{n=1}^{\infty} \frac{F_n b K_n^2}{2k_N \sin^4 k_N} \left\langle \boldsymbol{f}_1^N(y_1), \begin{bmatrix} \dfrac{\sinh(bK_n y_1)}{\sinh(K_n b)} \\ 0 \end{bmatrix} \right\rangle. \tag{2.32}$$

Therefore, each constant A_N or C_N can be expressed as a sum of the constants F_N and can be decoupled from any computations. Similar analysis of (2.27)–(2.28) but with

https://doi.org/10.1017/jfm.2013.99 Published online by Cambridge University Press

respect to the even eigenfunction $e_2^N(y_1)$ gives

$$B_N - D_N = \sum_{n=1}^{\infty} \frac{E_n \cos^2 K_n}{2\cos^4 K_N} \left\langle \boldsymbol{f}_2^N(y_1), \begin{bmatrix} \dfrac{\cosh(bK_n y_1)}{\cosh(bK_n)} \\ 0 \end{bmatrix} \right\rangle, \tag{2.33}$$

$$B_N + D_N \tanh\left(\frac{K_N}{b}\right) = -\sum_{n=1}^{\infty} \frac{E_n b K_n^2}{2K_N \cos^4 k_N} \left\langle \boldsymbol{f}_2^N(y_1), \begin{bmatrix} \dfrac{\cosh(bK_n y_1)}{\cosh(K_n b)} \\ 0 \end{bmatrix} \right\rangle. \tag{2.34}$$

The constants B_N and D_N can be expressed in terms of the constants E_n. Thus, the remaining (2.29)–(2.30) can be written as an infinite set of linear equations in E_n and F_n. An approximation of the solution is obtained by truncating the expansions to N_T terms and solving by substitution. The behaviour away from the sharp edges is captured by relatively few terms while accuracy at $(\pm 1, 0)$ is limited by a Gibbs phenomenon. Such truncations are justified by many authors, including Joseph (1977) and Joseph & Sturges (1978). We find that the error of the constants A_1, A_2 and B_1 in the expansion as N_T increases behaves as $\approx {N_T}^{-1.5}$. In addition, for large N we have $k_N \to (N + 1/4)\pi + \mathrm{i}\log(2N + 1/2)\pi$ and $K_N \to (N - 1/4)\pi + \mathrm{i}\log(2N - 1/2)\pi$. We therefore estimate that the truncated series for Ψ is valid except in circles centred at the shunt edges $(-1, 0)$ and $(1, 0)$ of radius $1/(N_T\pi + \pi/4)$. Results presented here are calculated with the truncation $N_T = 40$. The particular value is chosen by considering both the large computational cost of evaluating the $2 \times N_T^2$ integrals in the linear system of equations and the convergence rate of the series.

Figure 4 shows the streamfunction $\Psi(x, y)$ for $b = 1$. By construction, the flow is symmetric about both the x and y axes, and is from left to right in both channels. The flow is not parallel, as would be the case if the shunt were not there. In the vicinity of the shunt the flow is affected by the change in boundary condition: it is the second derivative of Ψ, not the first, that is zero along the shunt. The flow converges towards a plane Poiseuille profile on the length scale of the shunt width, as expected for low-Reynolds-number flows.

2.2. *Second solution (single-channel flow)*

The second solution we consider is characterized by plane Poiseuille flow in only one of the two channels. This breaks the symmetry in the flow about $y = 0$. Without loss of generality, we assume that it is the bottom channel that would have no inflow or outflow if the shunt were not present (figure 3*b*).

The boundary conditions are shown in figure 2, with $c_1 = 4b/3$, $c_2 = c_3 = c_4 = 0$. The flow is symmetric about $x = 0$, so it is sufficient to consider four subregions only (figure 5*a*,*c*). The expansions are similar to the those in the previous section:

$$\Psi_1(x, y_1) = f(y_1) + \sum_{n=1}^{\infty} \frac{A_n}{k_n^2} e_1^n(y_1) e^{k_n(x+1)/b} + \sum_{n=1}^{\infty} \frac{B_n}{K_n^2} e_2^n(y_1) e^{K_n(x+1)/b}, \tag{2.35}$$

$$\begin{aligned} \Psi_2(x, y_1) = f(y_1) &+ \sum_{n=1}^{\infty} \frac{E_n}{k_n^2} e_1^n(y_1) \frac{\cosh(k_n x/b)}{\cosh(k_n/b)} + \sum_{n=1}^{\infty} \frac{F_n}{K_n^2} e_2^n(y_1) \frac{\cosh(K_n x/b)}{\cosh(K_n/b)} \\ &+ \sum_{n=1}^{\infty} \frac{G_n}{b^2 K_n^2} \frac{\cosh(K_n b y_1)}{\cosh(K_n b)} e_2^n(x) + \sum_{n=1}^{\infty} \frac{H_n}{b^2 K_n^2} \frac{\sinh(K_n b y_1)}{\sinh(K_n b)} e_2^n(x), \end{aligned} \tag{2.36}$$

https://doi.org/10.1017/jfm.2013.99 Published online by Cambridge University Press

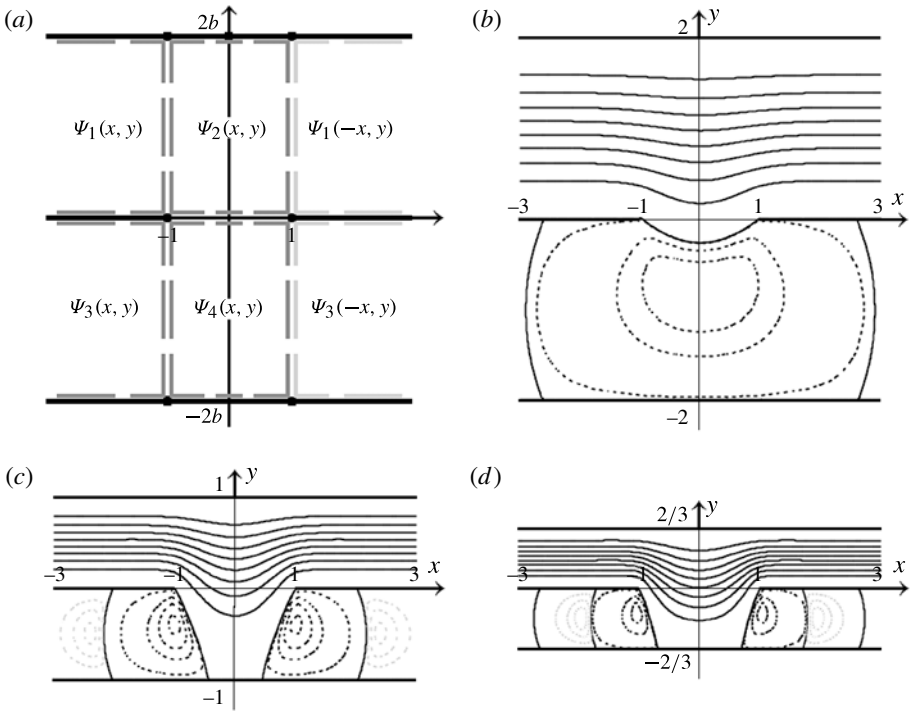


FIGURE 5. (*a*) A diagram of the subregions we consider when constructing the flow profile in figure 3(*b*). (*b*) Streamlines of the solution when $b = 1$; the solid contours correspond to $\Psi = (4/3) \times (n/9)$, $0 \leqslant n \leqslant 9$, and the dotted contours to $\Psi = -2 \times 10^{-4}$–$0.06 \times (n/4)$, $0 \leqslant n \leqslant 4$. (*c*) Streamlines when $b = 1/2$; the solid contours correspond to $\Psi = (4/3) \times (n/9)$, $0 \leqslant n \leqslant 9$, the dotted black contours to $\Psi = -6.4 \times 10^{-4}$–$6.4 \times 10^{-3} \times n$, $0 \leqslant n \leqslant 3$, and the dotted grey contours to $\Psi = 1.6 \times 10^{-5} + 2 \times 10^{-5} \times n$, $0 \leqslant n \leqslant 2$. (*d*) Streamlines when $b = 1/3$; the solid contours correspond to $\Psi = (4/3) \times (n/9)$, $0 \leqslant n \leqslant 9$, the dotted black contours to $\Psi = -8 \times 10^{-5}$–$8 \times 10^{-3} \times n$, $0 \leqslant n \leqslant 2$, and the dotted grey contours to $\Psi = 8 \times 10^{-6} + 1.8 \times 10^{-5} \times n$, $0 \leqslant n \leqslant 2$.

$$\Psi_3(x, y_2) = \sum_{n=1}^{\infty} \frac{C_n}{k_n^2} e_1^n(y_2) e^{k_n(x+1)/b} + \sum_{n=1}^{\infty} \frac{D_n}{K_n^2} e_2^n(y_2) e^{K_n(x+1)/b}, \tag{2.37}$$

$$\Psi_4(x, y_2) = \sum_{n=1}^{\infty} \frac{I_n}{k_n^2} e_1^n(y_2) \frac{\cosh(k_n x/b)}{\cosh(k_n/b)} + \sum_{n=1}^{\infty} \frac{J_n}{K_n^2} e_2^n(y_2) \frac{\cosh(K_n x/b)}{\cosh(K_n/b)} + \sum_{n=1}^{\infty} \frac{L_n}{b^2 K_n^2} \frac{\cosh(K_n b y_2)}{\cosh(K_n b)} e_2^n(x) + \sum_{n=1}^{\infty} \frac{M_n}{b^2 K_n^2} \frac{\sinh(K_n b y_2)}{\sinh(K_n b)} e_2^n(x), \tag{2.38}$$

where y_2 is defined in (2.14). There are 16 equations that need to be satisfied by these expansions. By construction, Ψ satisfies the boundary conditions on all rigid walls, apart from $\{x \in [-1, 1], y = 2b\}$ and $\{x \in [-1, 1], y = 2b\}$. These provide two equations for $\Psi_2(x, y)$ and two for $\Psi_4(x, y)$. There are also three interfaces that require continuity conditions. As before, the solutions on both sides of such interfaces are matched up

https://doi.org/10.1017/jfm.2013.99 Published online by Cambridge University Press

to the third derivative. This yields eight equations for the two interfaces at $x = -1$ and four equations at $y = 0$. Integration is performed for each eigenfunction as before. All constants decouple, apart from G_n, H_n, L_n and M_n. These form a system of linear equations that can be solved after truncation to N_T terms in each summation. For this case, we use the truncation number $N_T = 32$, which is chosen so that the computation costs associated with evaluating all of the integrals in the system of linear equations are the same as those associated with the first solution. The truncated approximation is again valid everywhere apart from at points closer than $1/(N_T\pi + \pi/4)$ to the shunt edges.

Plots of Ψ for $b = 1$, $b = 1/2$ and $b = 1/3$ are shown in figure 5. The contour lines in the top channel are uniformly spaced in the range $[0, 4b/3]$, whereas those in the lower channel are uniformly spaced in different ranges that are much lower in amplitude. The flow is dominated by the plane Poiseuille term, as expected. A relatively small amount of fluid crosses into the bottom channel: the streamline that joins the two edges of the shunt serves as the free boundary for the fluid in the two channels. There would be no flow in the bottom channel were it not for the shunt and the shear that the flow above exerts. The closed streamlines indicate that there are weak circulatory regions in the bottom channel, which are the Moffatt eddies that form in low-Reynolds-number flow in any corner of angle less than approximately 146° (Moffatt 1963) (our solution corresponds to a 'corner' of zero angle). Our analytical solution suggests that as x increases, the distance between the eddies converges towards a constant, which is determined by the imaginary part of the smallest root K_n or k_n, i.e. $\mathrm{Im}\{K_1\} \approx 1.1254$. The amplitude of the streamfunction inside the eddies decays exponentially as $\exp(-\mathrm{Im}\{K_1\}|x|/b)$ for large $|x|$; so the larger the shunt width is compared with the width of the channels (or the smaller b is), the higher the rate of decay. Moreover, as b decreases beyond $b <\approx 1/3$, the shunt width becomes comparable to the entrance length of flow in the wider channel and so the velocity distribution along $x = 0$ approaches a parabolic profile.

2.3. *Third solution (flow through the shunt)*

The third, and final, solution to be considered is represented by figure 3(*c*). Unlike the first two flows, it introduces flow of non-zero net flux through the shunt, which means that it is linearly independent of the previous solutions. In addition, it is symmetric about both the x and y axes. A solution can be obtained by considering two subregions of the geometry, as shown in figure 6. Note that this is the first decomposition where one region is of height $4b$ rather than $2b$, so that some eigenfunctions have argument $y_3 = y/2b$. This permits the plane Poiseuille flow term to be expanded as a linear combination of eigenfunctions. The boundary conditions associated with this third solution are shown in figure 2, where the constants are $c_1 = c_4 = 0$, $c_3 = -4b/3$ and $c_2 = 4b/3$.

The solutions in the two subregions can be represented in the following way:

$$\Psi_1(x, y_1) = f(y_1) - \frac{4b}{3} + \sum_{n=1}^{\infty} \frac{A_n}{k_n^2} e_1^n(y_1) e^{k_n(1-x)/b} + \sum_{n=1}^{\infty} \frac{B_n}{K_n^2} e_2^n(y_1) e^{K_n(1-x)/b}, \quad (2.39)$$

$$\Psi_2(x, y_3) = \sum_{n=1}^{\infty} \frac{C_n}{K_n^2} e_2^n(y_3) \frac{\sinh(K_n x/2b)}{\sinh(K_n/2b)}. \quad (2.40)$$

https://doi.org/10.1017/jfm.2013.99 Published online by Cambridge University Press

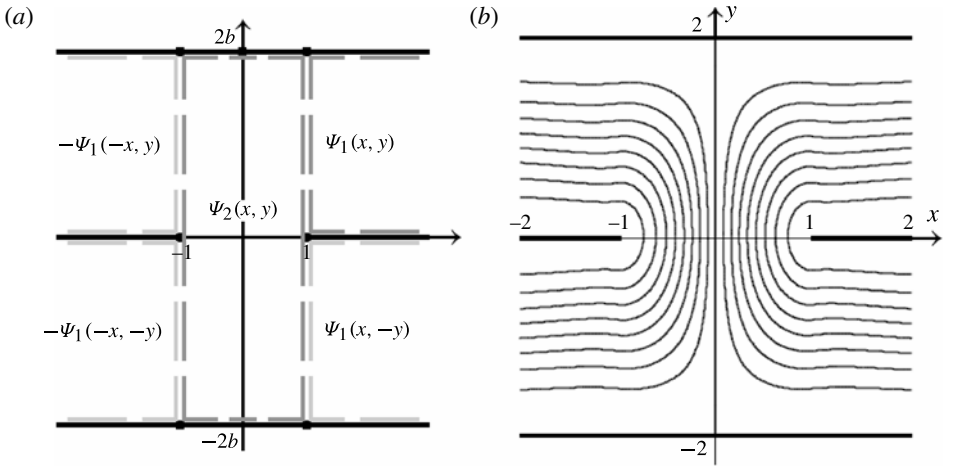


FIGURE 6. (*a*) A diagram of the subregions we consider when constructing the flow profile in figure 3(*c*). (*b*) Streamlines (from bottom to top) associated with the streamfunction Ψ when $b = 1$.

Note that there is no explicit plane Poiseuille flow term in the second expansion, and that the two expressions contain eigenfunctions that are biorthogonal over different regions, as indicated by the arguments y_1 and y_3. In addition, the chosen forms already consist of relatively few constants: 3, compared with 6 and 12 in the previous two sections (all boundary conditions are satisfied by the choice of expansion). As before, we match at the interface $x = 1$ to ensure the continuity of the streamfunction and its first three x-derivatives. This is equivalent to

$$\sum_{n=1}^{\infty} \frac{C_n}{K_n^2} e_2^n(y_3) = f(y_1) - \frac{4b}{3} + \sum_{n=1}^{\infty} \frac{A_n}{k_n^2} e_1^n(y_1) + \sum_{n=1}^{\infty} \frac{B_n}{K_n^2} e_2^n(y_1), \tag{2.41}$$

$$\sum_{n=1}^{\infty} \frac{C_n \coth(K_n/2b)}{2K_n} e_2^n(y_3) = -\sum_{n=1}^{\infty} \frac{A_n}{k_n} e_1^n(y_1) - \sum_{n=1}^{\infty} \frac{B_n}{K_n} e_2^n(y_1), \tag{2.42}$$

$$\sum_{n=1}^{\infty} \frac{C_n}{4} e_2^n(y_3) = \sum_{n=1}^{\infty} A_n e_1^n(y_1) + \sum_{n=1}^{\infty} B_n e_2^n(y_1), \tag{2.43}$$

$$\sum_{n=1}^{\infty} \frac{C_n K_n \coth(K_n/2b)}{8} e_2^n(y_3) = -\sum_{n=1}^{\infty} A_n k_n e_1^n(y_1) - \sum_{n=1}^{\infty} B_n K_n e_2^n(y_1). \tag{2.44}$$

As before, the biorthogonality condition is used to obtain a system of linear equations. There is one difference: this time the first two and last two equations are coupled together before integration. As suggested by Phillips (1989), the two equations that match the second and third derivatives of the streamfunction should be analysed with respect to the bases $e_1^n(y_1)$ and $e_2^n(y_1)$. Both Ψ and its first derivative are continuous at the edges of the shunt $(\pm 1, 0)$. Therefore, integration can be performed with respect to the eigenfunction $e_2^n(y_3)$. Equations (2.41)–(2.44) are first rewritten in vector form after

https://doi.org/10.1017/jfm.2013.99 Published online by Cambridge University Press

differentiation of (2.41) and (2.43):

$$\sum_{n=1}^{\infty}\frac{C_n}{4}\boldsymbol{e}_2^n(y_3)=\begin{bmatrix}0\\2by_1\end{bmatrix}+\sum_{n=1}^{\infty}\frac{C_n\left(K_n-2\coth\left(\dfrac{K_n}{2b}\right)\right)}{4K_n}\begin{bmatrix}e_2^n(y_3)\\0\end{bmatrix}$$
$$+\sum_{n=1}^{\infty}A_n\begin{bmatrix}-e_1^n(y_1)/k_n\\e_1^{n\prime\prime}(y_1)/{k_n}^2\end{bmatrix}+\sum_{n=1}^{\infty}B_n\begin{bmatrix}-e_2^n(y_1)/K_n\\e_2^{n\prime\prime}(y_1)/{K_n}^2\end{bmatrix}, \tag{2.45}$$

$$\sum_{n=1}^{\infty}A_n{k_n}^2\boldsymbol{e}_1^n(y_1)+\sum_{n=1}^{\infty}B_n{K_n}^2\boldsymbol{e}_2^n(y_1)$$
$$=\sum_{n=1}^{\infty}A_nk_n(k_n-1)\begin{bmatrix}e_1^n(y_1)\\0\end{bmatrix}+\sum_{n=1}^{\infty}B_nK_n(K_n-1)\begin{bmatrix}e_2^n(y_1)\\0\end{bmatrix}$$
$$+\sum_{n=1}^{\infty}\frac{C_n}{16}\begin{bmatrix}-2K_n\coth\left(\dfrac{K_n}{2b}\right)e_2^n(y_3)\\e_2^{n\prime\prime}(y_3)\end{bmatrix}. \tag{2.46}$$

Equation (2.45) is then premultiplied by the adjoint eigenvector corresponding to $\boldsymbol{e}_2^n(y/2b)$ and integration is performed over the range $y\in(0,2b)$. In addition, (2.46) forms two equations after similar integration with respect to the eigenvectors $e_1^n(y_1)$ and $e_2^n(y_1)$, respectively. This yields three infinite sets of linear equations for A_n, B_n and C_n. Figure 6 shows the streamlines of the flow when the summations are truncated to 20 terms. By construction, the solution is even in y and odd in x.

This third solution is a special case ($\alpha=0$) of the geometry considered by Cachile *et al.* (2012), in which the four channels meet at an angle α. Their numerical results suggest that, for small enough α, there will be at least three recirculation regions in the vicinity of the shunt. These disappear when $\alpha=0$, but they may be important when a side-to-side anastomosis connects non-parallel segments of the intestine.

Having found the solutions for three linearly independent cases, we can now derive the solution for any values of c_1, c_2, c_3 and c_4. First, we focus on the solutions that are relevant to modelling a side-to-side anastomosis.

3. Application: a side-to-side anastomosis in the gut

Side-to-side anastomoses can be created in the gut to divert a proportion of the total flux so that it bypasses diseased or highly resistive sections of the intestine. An example of the use of this treatment is in patients with Crohn's disease, for which a high proportion of fluid is shunted. The flow in the small intestine has a Reynolds number of the order of 10^{-3} and varies only slowly in time. Therefore, the method developed in this paper is applicable, and the solutions can be written as a superposition of those derived in §§ 2.1–2.3, each multiplied by a slowly varying function of time.

In this section, we focus on the flow properties as the fraction of flow through the shunt changes, since the size of the surgical cut during a side-to-side anastomosis is the main determinant of the volume fraction for the particular fluid that passes through the top channel. We first consider results calculated for the particular case when the width of the shunt L^d is the same size as the height of the channel, i.e. $L^d=1.25\times10^{-2}$ m, which is typical of cuts used during surgery.

https://doi.org/10.1017/jfm.2013.99 Published online by Cambridge University Press

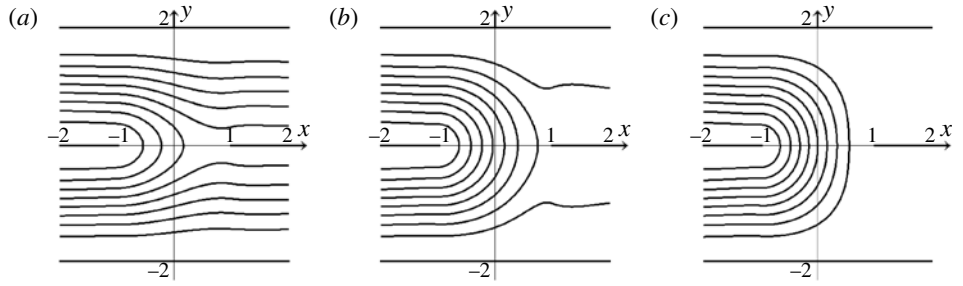


FIGURE 7. Streamlines of flow in a side-to-side anastomosis for different proportions of flow bypassing the intestinal loop over the net flow entering the domain through the top left extremity: (*a*) 40; (*b*) 80; (*c*) 100 %. Flow enters through the top left channel end and leaves through the bottom left channel end.

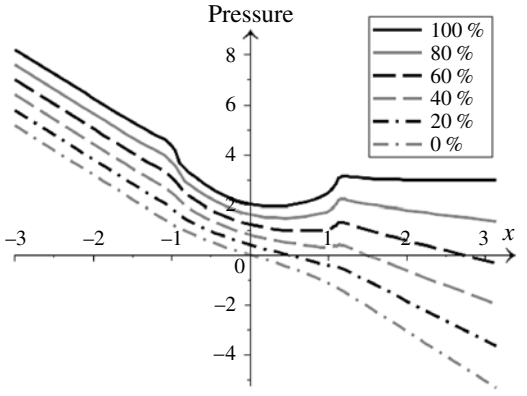


FIGURE 8. Pressure along the middle of the top channel when $b = 1$ for different flux ratios of flow through the shunt.

We assume that no fluid leaves the gut in the loop, and therefore the flux exiting the top right channel reenters through the bottom right channel in figure 1, meaning that $c_1 = c_4$, and we also normalize the maximum velocity at the inlet. The results are shown in figure 7 for various fluxes through the shunt: the first plot is for the case when 40 % of the flow bypasses the intestinal loop, and the last when the entire flow is diverted through the shunt.

Pressure is of interest to the clinician because it is linearly related to the flux and can be measured relatively easily clinically. The non-dimensional pressure along the middle of the top channel for varying shunt flows is shown in figure 8, where the pressure scale is $2\mu^d \tilde{U}^d/\tilde{L}^d$. The pressure curves are separated by an arbitrary integration constant. The pressure gradients are identical and tend to -2 as x^d approaches the inlet to the left. Downstream, the pressure gradients differ according to the bypass flow percentage, varying from -2 for 0 % to 0 for 100 %.

At the edges of the shunt, the streamfunction and velocity field in the Stokes flow solution are finite, but higher derivatives are singular. We use polar coordinates (r, θ) centred on the edge of the gap, where $\theta = \pm\pi$ is the wall. To leading order as $r \to 0$, $\psi \simeq Ar^{3/2}\cos^2(\theta/2)\sin[(\theta - \alpha)/2]$, where A and α are constants determined

https://doi.org/10.1017/jfm.2013.99 Published online by Cambridge University Press

globally. Thus, a streamline can leave the edge at any angle $\theta = \alpha$, while the pressure, vorticity and shear stress are proportional to $r^{-1/2}$ to leading order. The amplitude A varies exactly linearly with the flux through the shunt; it increases at the edge $x = -1$ and decreases at the edge $x = 1$. The series solution converges only slowly near the singularities, meaning that many terms are required to predict the behaviour near there accurately.

The analytical model can be used to compare the flow for different shunt widths. We present results for the change in flow profile with respect to this width when the flux through the shunt is zero (figure 9*a*) and when the flux through the intestinal bend equals that diverted through the anastomosis, i.e. when the flux ratio $= 50\,\%$ (figure 9*b*). The second figure in the second column ($b = 1$) illustrates a typical desired outcome, where almost all of the flow passes either through the shunt or round the loop. As the width b decreases, however, a substantial closed circulatory region develops in the loop, as shown in the lower two plots in the second column. The fluxes in this region are estimated to be $0.2, 20.4$ and $40.8\,\%$ of the inlet total flux for the values $b = 1$, $b = 1/2$ and $b = 1/3$, respectively. Circulatory regions are potentially damaging to the tissue either by increasing the residence time of toxins or by facilitating the development of infection in the loop. Thus the acceleration in weight loss must be balanced against increased health risk.

The results for the case of no net flux through the shunt reveal a similar effect: as the shunt width increases, the zero net flux is maintained by two counter-rotating disconnected loops. The flux in these loops increases as b decreases again. The flow profiles in this first column can be obtained by superimposing the solution found in § 2.2 and its inverted image in the opposite direction. When the shunt is large, the plane Poiseuille profile entering the top channel has sufficient distance to develop into plane Poiseuille flow spanning the wider channel. Then the inverted profile added there results in cancellation of flow along and near the line $x = 0$, and thus also in the aforementioned recirculating regions to the right of the anastomoses. If there are multiple such large shunts, then we expect that multiple recirculating regions will also occur. This concurs with many clinical observations that multiple smaller anastomoses are more successful than a single larger one.

4. Conclusion and discussion

Flow in the gut is not very well understood due to difficulties in measurements. Although abdominal surgical procedures are becoming increasingly widespread, there is a wide range of surgical procedures, and subjective preference, experience and available resources often dictate the choice of surgery rather than more scientific criteria. The model derived in this paper is intended as a first step towards understanding and predicting the characteristics of one particular procedure, a side-to-side anastomosis. The analytical form of the solution allows us to investigate different parameters and regimes. It provides estimates for the velocity and pressure distributions in the small intestine based on an idealized two-dimensional geometry of a shunt, and therefore has the potential to be applied in the future to optimize key factors in surgery such as the position, size and resistance of shunts. Such models are important for the future success of invasive treatments.

Our emphasis on the side-to-side anastomosis means that we have not exhausted all linear combination of the three solutions derived in this paper. The model can be applied to other biological problems where low-Reynolds-number flow is shunted or leaks through a gap. For example, a similar two-dimensional geometry was considered

https://doi.org/10.1017/jfm.2013.99 Published online by Cambridge University Press

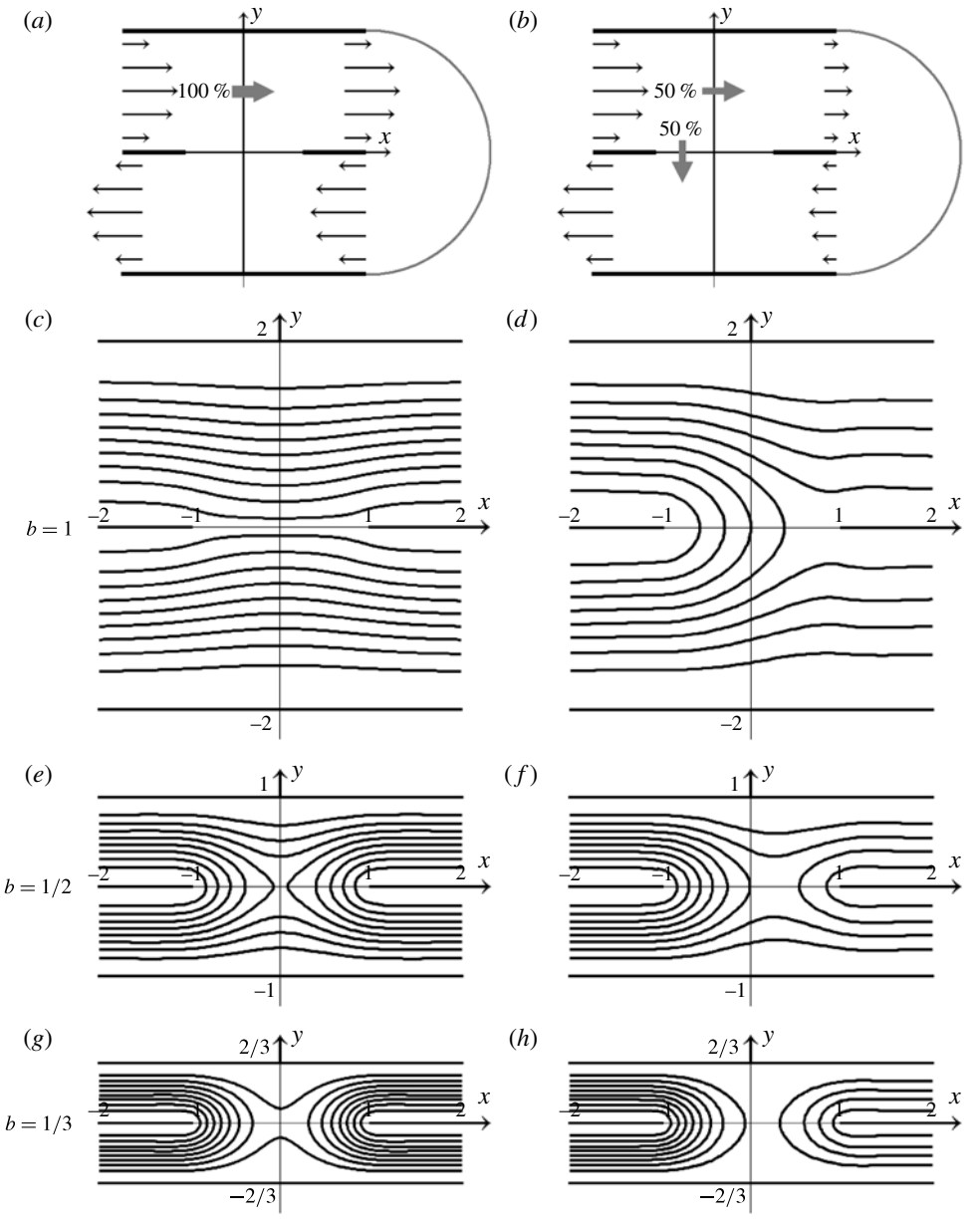


FIGURE 9. (*a*,*b*) Schematic drawings of flow round an intestinal bend when there is no net flux through the shunt (*a*) and when 50 % of the total flux entering the intestine through the top left channel is bypassed through the shunt (*b*). The plots below the drawings correspond to streamlines of the flows with such flow distribution when (*c*,*d*) $b = 1$, (*e*,*f*) $b = 1/2$ and (*g*,*h*) $b = 1/3$. Note the closed circulation loops in the bend for $b = 1/2$ and $b = 1/3$.

by Adamson & Michel (1993) for the flow through a discontinuity in the tight junction of an intercellular cleft. In addition, the mathematical model can be easily modified by imposing the closure of some of the channel ends to simulate any problem where low-Reynolds-number flow in one main channel leaks through a gap on one of the

https://doi.org/10.1017/jfm.2013.99 Published online by Cambridge University Press

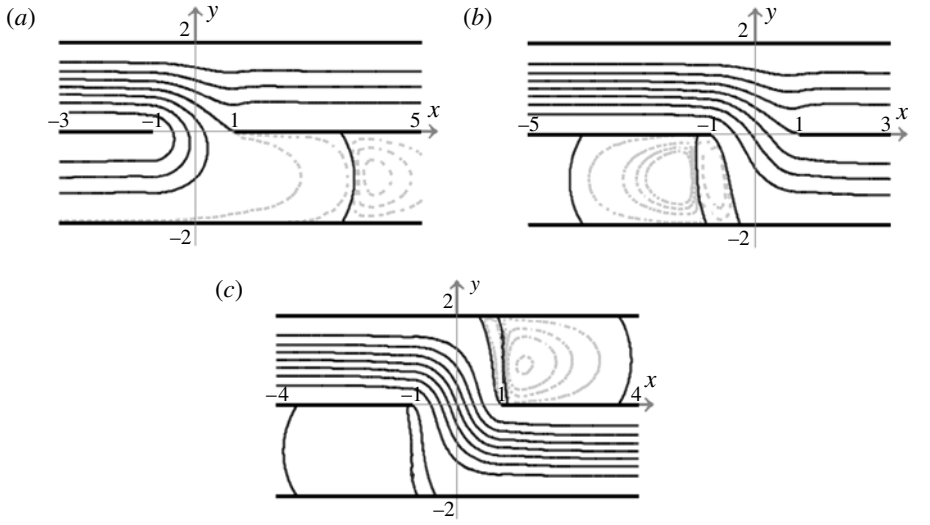


FIGURE 10. Flow streamlines when $b = 1$ if one channel end is blocked (*a*,*b*) and if two diagonal channel ends are closed (*c*). Flow enters through the top left channel end and leaves through the bottom left channel end in all three plots. The solid contours correspond to $\Psi = (4/3) \times (n/8)$, $0 \leqslant n \leqslant 8$. (*a*) The dotted grey contours correspond to $\Psi = 2/3 - 5 \times 10^{-3}, 2/3 - 10^{-4}$ and $\Psi = 2/3 + 10^{-5}, 2/3 + 3 \times 10^{-5}, 2/3 + 6 \times 10^{-5}$. (*b*) The dotted grey contours correspond to $\Psi = -5 \times 10^{-3}, -10^{-3}$ and $\Psi = 10^{-4}, 10^{-3}, 1.9 \times 10^{-3}, 2.8 \times 10^{-3}$. (*c*) The dotted grey contours correspond to $\Psi = 4/3 + 2 \times 10^{-3}$ and $\Psi = 4/3 - 10^{-3}, 4/3 - 5 \times 10^{-3}, 4/3 - 10^{-2}, 4/3 - 2 \times 10^{-2}$.

walls or into a single vessel. Such examples include Schlemm's canal in the eye and mixing channels in microfluidics. Other combinations of the three solutions in the model can be used to model the microvascular networks in the brain and, in particular, many of the redundant loops. Figure 10 shows three possible linear combinations when there is no flow in or out of some of the channel extremities, which can be used to model low-Reynolds-number flows with a blocked vessel a long way away from the shunt. The solutions (*a*), (*b*) and (*c*) correspond to the choices $\{4/3, 0, 2/3, 2/3\}$, $\{4/3, 0, 2/3, 0\}$ and $\{4/3, 0, 4/3, 0\}$ for $\{c_1, c_2, c_3, c_4\}$ in figure 2, respectively. The thin regions of circulation in the vicinity of a sharp corner are consistent with the results found by Cachile *et al.* (2012).

In this paper we have considered low-Reynolds-number flow in a two-dimensional geometry of two channels joined by a finite-sized shunt. Although the problem is readily solved numerically for a particular geometry, the analytical approach provides a solution for the entire range of values of b. The difficulty in studying this problem analytically is that a general solution of the biharmonic equation cannot be expressed using a single orthogonal basis of eigenfunctions. Progress is made by decomposing the domain into rectangular regions and considering Papkovich–Fadle expansions in each one. This method is usually used for geometries with only one inlet and one outlet, and therefore the solutions in this paper are a natural extension to previous work. The methodology required to obtain the third solution in this paper is of particular interest, since it uses two different bases in each rectangular region.

https://doi.org/10.1017/jfm.2013.99 Published online by Cambridge University Press

Acknowledgements

The authors would like to thank Professor T. Phillips from Cardiff University for his invaluable help and many discussions on the theory of this paper. We are also grateful to S. Llewellyn-Smith for his elucidation of a possible Wiener–Hopf approach to this problem.

REFERENCES

ABRAHAMS, I. D., DAVIS, A. M. J., SMITH, S. & LLEWELLYN, G. 2008 Asymmetric channel divider in Stokes flow. *SIAM J. Appl. Maths* **68** (5), 1439–1463.

ADAMSON, R. H. & MICHEL, C. C. 1993 Pathways through the intercellular clefts of frog mesenteric capillaries. *J. Physiol.* **466**, 303–327.

BUCHWALD, V. T. & DORAN, H. E. 1965 Eigenfunctions of plane elastostatics. II. A mixed boundary value problem of the strip. *Proc. R. Soc. Lond.* A **284**, 69–82.

CACHILE, M., TALON, L., GOMBA, J. M., HULIN, J. P. & AURADOU, H. 2012 Stokes flow paths separation and recirculation cells in x-junctions of varying angle. *Phys. Fluids* **24** (021704), 1–7.

CROWDY, D. & SAMSON, O. 2010 Stokes flows past gaps in a wall. *Proc. R. Soc. Lond.* A **466** (2121), 2727–2746.

DAVIS, A. M. J. 1991 Shear flow disturbance due to a hole in the plane. *Phys. Fluids* **3** (3), 478–480.

DRIESEN, C. H., KUERTEN, J. G. M. & STRENG, M. 1998 Low-Reynolds-number flow over partially covered cavities. *J. Engng Maths* **34** (1–2), 3–20.

FOOTE, R. M. L. & BUCHWALD, V. T. 1985 An exact solution for the stress intensity factor for a double cantilever beam. *Int. J. Fracture* **29**, 125–134.

JOSEPH, D. D. 1977 The convergence of biorthogonal series for biharmonic and Stokes flow edge problems. Part I. *SIAM J. Appl. Maths* **33** (2), 337–347.

JOSEPH, D. D. & STURGES, L. 1975 The free surface on a liquid filling a trench heated from its side. *J. Fluid Mech.* **69**, 565–590.

JOSEPH, D. D. & STURGES, L. 1978 The convergence of biorthogonal series for biharmonic and Stokes flow edge problems. Part II. *SIAM J. Appl. Maths* **34** (1), 7–26.

JOSEPH, D. D., STURGES, L. D. & WARNER, W. H. 1982 Convergence of biorthogonal series of biharmonic eigenfunctions by the method of Titchmarsh. *Arch. Rat. Mech. Anal.* **78**, 223–279.

JOYCE, M., SWEENEY, K. J., JOHNSTON, S. & GERAGHTY, J. G. 2002 Techniques of bowel resection and anastomosis. *CME J. Gynecol. Oncol.* **7**, 284–289.

KIM, M. U. & CHUNG, M. K. 1984 Two-dimensional slow viscous flow past a plate midway between an infinite channel. *J. Phys. Soc. Japan* **53** (1), 156–166.

KIM, S. & KARRILA, S. J. 2005 *Microhydrodynamics: Principles and Selected Applications*, 2nd edn. Dover.

KIRAN, R. P., NISAR, P. J., CHURCH, J. M. & FAZIO, V. W. 2011 The role of primary surgical procedure in maintaining intestinal continuity for patients with Crohn's colitis. *Ann. Surg.* **253** (6), 1130–1135.

KO, H.-J. & JEONG, J.-T. 1994 Two-dimensional slow stagnation flow near a slit. *J. Phys. Soc. Japan* **63** (9), 3288–3294.

MOFFATT, H. K. 1963 Viscous and resistive eddies near a sharp corner. *J. Fluid Mech.* **18** (1), 1–18.

PHILLIPS, T. N. 1989 Singular matched eigenfunction expansions for Stokes flow around a corner. *IMA J. Appl. Maths* **42** (1), 13–26.

POZRIKIDIS, C. 1992 *Boundary Integral and Singularity Methods for Linearized Viscous Flow*, 1st edn. Cambridge University Press.

RESEGOTTI, A., ASTEGIANO, M., FARINA, E. C., CICCONE, G., AVAGNINA, G., GIUSTETTO, A., CAMPRA, D. & FRONDA, G. R. 2005 Side-to-side stapled anastomosis strongly reduces anastomotic leak rates in Crohn's disease surgery. *Dis. Colon Rectum* **48** (3), 464–468.

https://doi.org/10.1017/jfm.2013.99 Published online by Cambridge University Press

SETCHI, A. 2012 Mathematical modelling of flow through shunts: application to patent ductus arteriosus and side-to-side anastomosis. PhD thesis, Imperial College London.

SETCHI, A., MESTEL, A. J., SIGGERS, J. H., PARKER, K. H., TAN, M. W. & WANG, K. 2012 Mathematical model of flow through the patent ductus arteriosus. *J. Math. Biol.* doi:10.1007/s00285-012-0596-8.

SMITH, R. C. T. 1952 The bending of a semi-infinite strip. *Austral. J. Sci. Res.* **5**, 227–237.

SMITH, S. H. 1987 Stokes flow past slits and holes. *Intl J. Multiphase Flow* **13**, 219–231.

SOUBA, W. W., FINK, M. P., JURKOVIC, G. J., PEARCE, W. H., PEMBERTON, J. H. & SOPER, N. J. (Eds) 2007 *ACS Surgery: Principles and Practice*, 6th edn. Decker Publishing, Particular contribution by N. J. Mortensen and S. Ashraf in Chapter 5.29, Intestinal Anastomosis. Image available at http://206.47.151.137/bcdecker/figures/acs/thumb/part05_ch29_fig5.gif (accessed 23 July 2012).

TRIPATHI, D. 2011 A mathematical model for the peristaltic flow of chyme movement in small intestine. *Math. Biosci.* **233** (2), 90–97.

TROGDON, S. A. & JOSEPH, D. D. 1982 Matched eigenfunction expansions for a slow flow over a slot. *J. Non-Newtonian Fluid Mech.* **10**, 185–213.

https://doi.org/10.1017/jfm.2013.99 Published online by Cambridge University Press